Lamellar-structured low-cost $FeMn_{0.7}Ni_{0.6}Cr_{0.4}Al_{0.3}$ high entropy alloy with excellent tensile properties

Zhenfei Jiang [a,b], Weiping Chen [a], Chenliang Chu [a], Zhiqiang Fu [a,*], Yemao Lu [b,**], Yulia Ivanisenko [b]

[a] Guangdong Key Laboratory for Advanced Metallic Materials Processing, South China University of Technology, Guangzhou, Guangdong, 510640, China
[b] Institute of Nanotechnology, Karlsruhe Institute of Technology (KIT), D-76021, Karlsruhe, Germany

ARTICLE INFO

Keywords:
High entropy alloys
Casting
Lamellar
Precipitate
Mechanical properties

ABSTRACT

High-performance structural materials with low cost are highly desirable yet challenging. Here we report a novel Co-free $FeMn_{0.7}Ni_{0.6}Cr_{0.4}Al_{0.3}$ high entropy alloy (HEA) possessing *in situ*-formed lamellar structure fabricated by a vacuum arc melting method. The alloy is composed of alternating disordered face centered cubic (FCC) lamellae and disordered body centered cubic (BCC) lamellae, with a few ordered BCC (B2) precipitates embedded in the FCC matrix and a high-density B2 precipitates embedded in the BCC matrix. The composite-like lamellar structure renders this as-cast alloy with extraordinary tensile properties with a yield strength of ~635 MPa and an ultimate tensile strength of ~1061 MPa, together with an elongation of ~19.4% at room temperature, primarily ascribing to the lamellar boundary strengthening. This as-cast cost-effective $FeMn_{0.7}Ni_{0.6}Cr_{0.4}Al_{0.3}$ alloy with lamellar structure and outstanding tensile properties is highly suitable for manufacturing high-performance metallic products by direct casting.

1. Introduction

The requirements for high-performance structural materials have become urgent along with scientific and technological innovation. The emergence of high-entropy alloys (HEAs), with no single dominant element in contrary to conventional dilute alloys, has opened up the broad compositional space for the discovery of new alloys and unprecedented properties [1–4]. By utilizing this unconventional alloying design concept, a wide variety of novel HEAs with exceptional mechanical and physical properties have been continuously explored over the past decade [4–6]. For instance, Li et al. designed a non-equiatomic CoFeNiTaAl HEA with a tensile strength of 1336 MPa combined with an elongation of 54%, high electrical resistivity of 103 μΩ cm, and extremely low coercivity of 78 A m^{-1} [4]. The precipitate-hardening $(CoFeNi)_{86}Al_7Ti_7$ HEA consisting of a disordered FCC matrix and high amount of ordered FCC nanoprecipitates presents an extraordinary balance between tensile strength and ductility [6]. However, almost all the available HEAs with high-performance contain high content of Co element, which is a strategic material and quite expensive compared with other elements, accordingly restricting their actual industrial application seriously [7,8].

Therefore, some researchers have developed a series of Co-free FeMnNiCrAl-based HEAs recently [7–12]. For instance, the coherent nanoprecipitates strengthened $Ni_{47-x}Fe_{30}Cr_{12}Mn_8Al_xTi_3$ and $(FeNi)_{67}Cr_{15}Mn_{10}Al_{8-x}Ti_x$ HEAs prepared by thermomechanical treatments display excellent strength-ductility synergy [8,9]. Wu et al. designed a low-cost $Fe_{40}Mn_{10}Ni_{25}Cr_{25}$ HEA with partially recrystallized heterogeneous microstructure and good combinations of high yield strength (~710 MPa) and good ductility (~18%) [10]. Nevertheless, it has been found that the tensile properties of the as-cast FeMnNiCrAl HEAs are still not acceptable up to now. The as-cast non-equiatomic FeMnNiCrAl HEAs with a single FCC phase exhibit outstanding ductility but extremely low yield strength [8–10]. Whereas some BCC-structured HEAs ($Fe_{36}Mn_{21}Cr_{18}Ni_{15}Al_{10}$ [11], $Al_{0.5}FeMnNiCrCu_{0.5}$ [12]) are characterized by their ultra-high compressive strength but insufficient ductility at room temperature. Recent studies suggest that establishing a dual-phase or multi-phase structure is an effective approach to improve the mechanical properties of high entropy alloys [13–15]. For example, with the addition of Ni to the $AlCoCrFeTi_{0.5}$ HEAs, FCC/BCC (A2+B2) multi-phase structure was obtained in the newly developed alloys and

* Corresponding author.
** Corresponding author.
E-mail addresses: zhiqiangfu2019@scut.edu.cn (Z. Fu), Yemao.Lu@partner.kit.edu (Y. Lu).

exhibited enhanced compressive strength [13]. The $AlCoCrFeNi_{2.1}$ eutectic HEA developed by Lu et al., consisting of alternating lamellar FCC/B2 structure, exhibited an ultimate tensile strength of ~1040 MPa with an elongation of ~17.1% in the as-cast state [15].

In this study, we developed a novel Co-free $FeMn_{0.7}Ni_{0.6}Cr_{0.4}Al_{0.3}$ HEA based on previously reported BCC-structured $Fe_{36}Mn_{21}Ni_{15}Cr_{18}Al_{10}$ HEA. In our design, different from the widely used alloy design strategies of varying the Al concentration, we modulate the phase proportion and microstructure by increasing the ratio of Ni/Cr aiming at obtaining FCC + BCC dual-phase microstructure. Comprehensive microstructure characterization and analysis of mechanical properties revealed that the studied alloy shows a novel *in situ*-formed lamellar structure and exhibits an excellent combination of high tensile strength and ductility.

2. Experimental

The $FeMn_{0.7}Ni_{0.6}Cr_{0.4}Al_{0.3}$ ($Fe_{33.33}Mn_{23.33}Ni_{20}Cr_{13.34}Al_{10}$ in at. %) HEA ingots were fabricated by vacuum arc melting using the mixtures of Fe, Mn, Ni, Cr, and Al metal pieces (purities >99.8 wt%) as starting materials under a high-purity argon atmosphere. The ingots were flipped over and remelted five times with electromagnetic stirring to ensure chemical homogeneity. The melt was then drop-casted into a copper mold with dimensions of 70 × 10 × 10 mm^3 by gravity. The crystal structures were detected by X-ray diffraction (XRD, PANalytical X'Pert Powder) using Cu Kα radiation in 2θ range from 20° to 100°. The microstructure morphology was observed using a Zeiss Auriga 60 scanning electron microscope (SEM) in backscatter electron (BSE) mode. SEM samples were polished down to 7000-grit SiC paper and followed by electrochemical polishing with a direct voltage of 20 V at 253 K. The transmission electron microscopy (TEM) analysis was conducted on FEI Titan Themis-Z equipped with double aberration correctors. The high angle annular dark field scanning TEM (HAADF-STEM) and electron energy-loss spectroscopy (EELS) were conducted to investigate the elemental distributions. Dog-bone tensile specimens were fabricated by electrical discharge machining with a gauge length of 10 mm, a thickness of ~1.1 mm, and a width of ~3 mm. Uniaxial tensile tests were performed on a Zwick/Roell Z020 universal testing machine with a nominal strain rate of 1×10^{-3} s^{-1} at ambient temperature. The strain was calibrated using a mechanical extensometer and four samples were tested to ensure reliability.

3. Result and discussion

The XRD pattern shown in Fig. 1(a) suggests that the as-cast $FeMn_{0.7}Ni_{0.6}Cr_{0.4}Al_{0.3}$ HEA is primarily composed of FCC and BCC/B2 phases. The low-angle superlattice diffraction peak at 2θ of 30.92° is attributed to the (100) planes of the ordered BCC (B2) phase, indicating that partial or entire BCC phase exhibit B2 structure. Fig. 1(b) shows a representative low-magnification BSE image, revealing that the as-cast $FeMn_{0.7}Ni_{0.6}Cr_{0.4}Al_{0.3}$ HEA exhibits an alternating lamellar microstructure. A further observation from the high-magnification BSE image (Fig. 1(c)) shows that there are two kinds of lamellae with different morphologies and contrast, i.e., bright lamellae with high-density precipitates and gray lamellae with a few precipitates. A statistical analysis using ImageJ software shows that, the thickness of bright lamellae and gray lamellae are estimated to be ~1.08 μm and ~1.36 μm, and their corresponding contents are ~44.26 vol% and ~55.74 vol%, respectively.

TEM investigation results of the as-cast $FeMn_{0.7}Ni_{0.6}Cr_{0.4}Al_{0.3}$ HEA are displayed in Fig. 2. The bright-field (BF) TEM image presented in Fig. 2(a) further confirms the *in-situ* lamellar composite-like solidification microstructure, consisting of two distinctly different lamellae. The microstructure of lamellae I contains high-density of precipitates, while a few precipitates are embedded in lamellae II. The corresponding selected area electron diffraction (SAED) patterns presented in Fig. 2(b) and (c) show that the matrixes of lamellae I and lamellae II are disordered BCC and disordered FCC phases, respectively. The SAED patterns of precipitates in BCC lamellae and precipitates in FCC lamellae are shown in Fig. 2(d) and (e), respectively. The presence of superlattice reflections indicates that the two kinds of precipitates both are ordered BCC (B2) structure. The size distribution and volume fraction of the B2-structured precipitates were estimated from the high-angle annular dark-field scanning transmission electron microscopy (HAADF-STEM) images containing more than 200 particles *via* ImageJ software. A representative HAADF-STEM image at a relatively low-magnification is shown in Fig. 2(f). The volume fractions of B2 precipitates in the FCC and BCC lamellae were estimated to be ~5.0 vol% and ~22.2 vol%, respectively. The size distribution of B2 precipitates in the FCC and BCC lamellae are plotted in Fig. 2(g) and (h), of which the average precipitate diameters are ~278 nm within FCC lamellae and ~332 nm within BCC lamellae.

Fig. 3 displays the HAADF-STEM micrograph and corresponding electron energy-loss spectroscopy (EELS) maps for the individual elements of Al, Cr, Mn, Fe, and Ni in the current alloy. According to the EELS maps and EDS/TEM results (as shown in Table 1), the BCC-structured matrix of lamellae I contains higher contents of Fe (~41.61 at.%) and Cr (~30.81 at.%), while the precipitates are enriched in Ni (~37.79 at.%) and Al (~26.51 at.%), which is consistent with high contents of Al and Ni favoring the formation of B2 phase in HEAs [11,16,17]. In lamellae II, the FCC-structured matrix is depleted in Al (~4.32 at.%) and Cr (~9.81 at.%), whereas the precipitates are likely to have similar chemical compositions to those of the precipitates embedded in the BCC lamellae.

Fig. 4(a) displays the typical engineering (red line) and true (blue line) tensile stress-strain curve of the as-cast $FeMn_{0.7}Ni_{0.6}Cr_{0.4}Al_{0.3}$ specimens. The engineering 0.2% offset yield strength ($\sigma^e_{0.2}$), ultimate tensile strength (σ^e_{UTS}), and total elongation (El^e) were ~635 ± 12 MPa, ~1061 ± 23 MPa, and ~19.5 ± 0.9%, respectively, revealing that the lamellar-type microstructure renders the alloy with an excellent combination of strength and ductility. When the engineering stress-strain curve was converted into a true stress-strain curve, the calculated true yield strength ($\sigma^t_{0.2}$), true ultimate tensile strength (σ^t_{UTS}), and uniform elongation (El^t) are ~641 MPa, ~1266 MPa and ~17.8%, respectively. The strength difference between σ^e_{UTS} and $\sigma^e_{0.2}$ is as high as 426 MPa (i.e., $\sigma^e_{UTS} - \sigma^e_{0.2} = 426$ MPa), and the σ^t_{UTS} is near twice the $\sigma^t_{0.2}$ in the as-cast

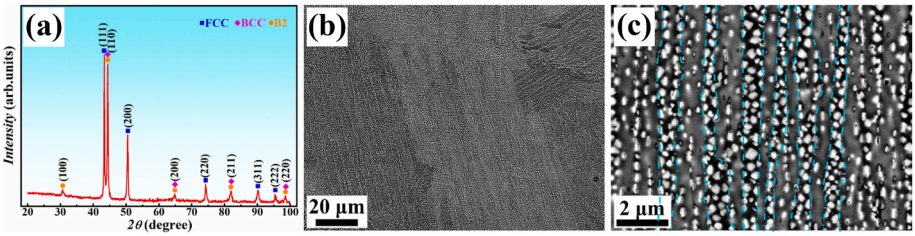

Fig. 1. XRD and SEM analyses for the as-cast $FeMn_{0.7}Ni_{0.6}Cr_{0.4}Al_{0.3}$ HEA. (a) XRD pattern showing the phase composition, (b) Representative low-magnification BSE image, (c) High-magnification BSE image.

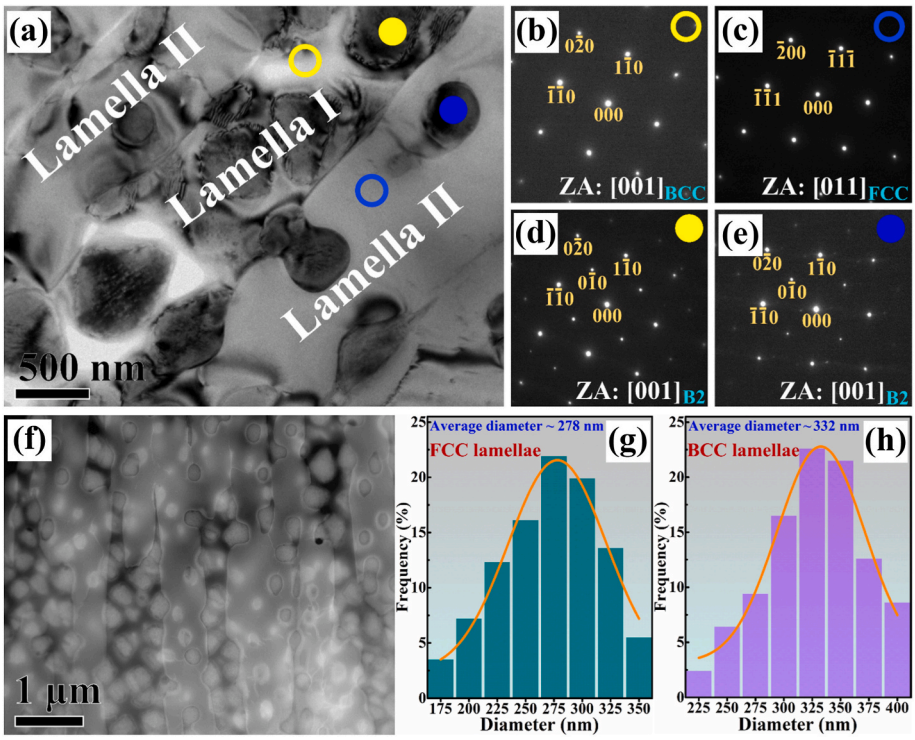

Fig. 2. TEM characterization of the as-cast $FeMn_{0.7}Ni_{0.6}Cr_{0.4}Al_{0.3}$ HEA. (a) Bright field TEM image, (b–e) Corresponding SAED patterns of phases in current alloy, (f) HAADF-STEM image. (g) Size distribution of precipitates dispersed in FCC lamellae, (h) Size distribution of precipitates dispersed in BCC lamellae.

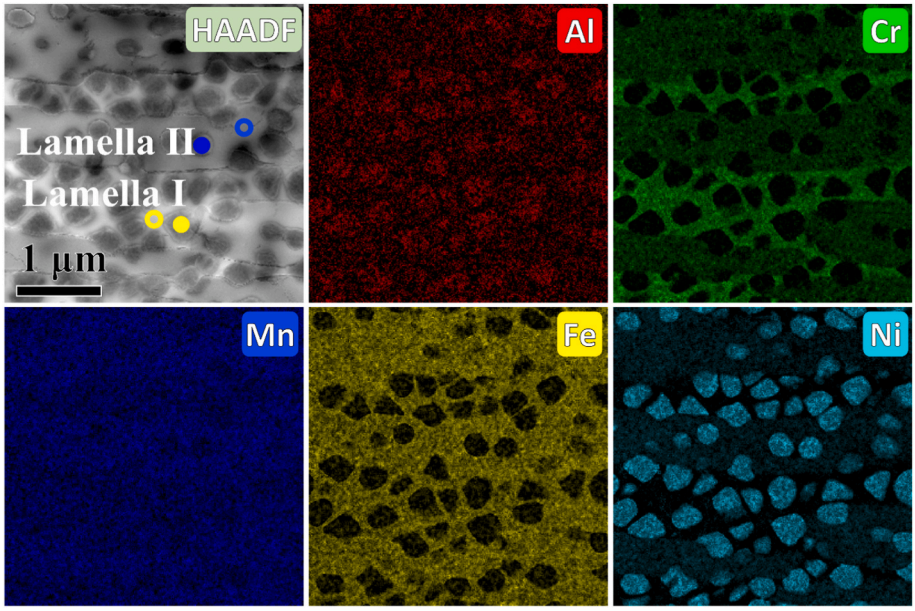

Fig. 3. HAADF-STEM image and corresponding EELS maps for the individual elements of Al, Cr, Mn, Fe, and Ni, respectively.

$FeMn_{0.7}Ni_{0.6}Cr_{0.4}Al_{0.3}$ alloy, implying an extraordinary strain-hardening capability that accounts for the observed high tensile strength and good ductility. The strain-hardening rate (SHR) by differentiating the true stress over true strain during tensile deformation was obtained to analyze the strain hardening quantitatively. The resulting SHR ($d\sigma^t/d\varepsilon^t$) versus true strain (ε^t) curve shown in Fig. 4(b) displays a typical three-stage hardening behavior with the increase of strain, as widely observed in other as-cast metallic materials [15,18]. In the first stage ($\varepsilon^t < 3.2\%$), the SHR first presents a dramatic drop. And then, the SHR slightly decreases from 5.6 GPa to 1.7 GPa in the wide ε^t range of 3.2%–17.1% in the second stage, which is a prerequisite for excellent tensile ductility. Finally, in the third stage, the SHR shows a sharp reduction until tensile neckdown, which usually is attributed to the exhausted deformability of alloys [18,19].

Previous research on the lamellar structured FCC/B2 HEAs revealed that dislocations initially engage upon propagation within the soft FCC lamellae, and initial plastic deformation occurs only in the FCC lamellae, since the FCC phases are notably softer than the BCC phases [18,20–22]. Hence, the parameter controlling the total yield strength is the thickness and physical properties of soft FCC lamellae [20,21]. It should be noted

Table 1
Chemical compositions obtained *via* TEM-EDS (in at.%) and volume fraction (%) of different phases in as-cast $FeMn_{0.7}Ni_{0.6}Cr_{0.4}Al_{0.3}$ HEA.

Regions	Al	Cr	Mn	Fe	Ni	Volume fraction (%)
Nominal	10.00	13.33	23.33	33.34	20.00	–
Matrix of FCC lamellae	4.32	9.81	24.83	40.92	20.12	50.7
Precipitates in FCC lamellae	25.84	5.12	18.92	13.61	36.51	5.0
Matrix of BCC lamellae	2.53	30.81	23.53	41.61	1.52	22.1
Precipitates in BCC lamellae	26.51	4.33	20.24	11.13	37.79	22.2

that the strengthening mechanisms in most metallic materials are summarized into four categories: dislocation hardening ($\Delta\sigma_D$), grain-boundary hardening ($\Delta\sigma_G$), solid-solution hardening ($\Delta\sigma_S$), and particles hardening ($\Delta\sigma_P$), which are considered to operate independently [23]. So, the yield strength of FCC lamellae can be evaluated as:

$$\sigma_{0.2} = \sigma_0 + \Delta\sigma_D + \Delta\sigma_G + \Delta\sigma_S + \Delta\sigma_P$$

where $\sigma_0 = 125$ MPa is the lattice friction strength, which is adopted from the widely cited equiatomic FeMnNiCoCr HEA [24]. $\Delta\sigma_D$ is the strength contribution from dislocation hardening, which usually is ignored for as-cast alloys [12]. It was documented that the classical Hall-Petch relationship also describes the yield strength of lamellar structures [20–22]. Based on the Hall-Petch modeling, the lamellar boundaries strengthening could be evaluated by $\Delta\sigma_G = k(\lambda)^{-1/2}$, where $k = 494$ MPa $\mu m^{1/2}$ is the Hall-Petch coefficient taken from the FeMnNiCoCr HEA [24] and $\lambda = 1.36$ μm is the average thickness of FCC lamellae. Therefore, the strengthening of FCC/BCC lamellar boundaries to the yield strength can be calculated as $\Delta\sigma_G = 423.6$ MPa, which provides the dominant contribution to the macroscopic yield strength.

For the FeMnNiCrAl alloy system, the Al atom has a larger atomic radius (0.143 nm), while the atomic sizes of Fe, Mn, Ni, and Cr are very close (~0.124 nm), and thus Al is simply treated as the solute in the FeMnNiCr solvent matrix to evaluate the strength enhancement caused by solid-solution hardening. The value of solid-solution strengthening induced by Al is expressed as [23]:

$$\Delta\sigma_S = M \cdot G \cdot \varepsilon_S^{3/2} \frac{c^{1/2}}{700}$$

in which $M = 3.06$ is the Taylor factor [23,25], $G = 46.78$ GPa is the shear modulus of Al [23], $c = 4.32\%$ is the concentration of Al in FCC phase (see Table 1), and ε_S is the interaction parameter expressed by the following equation:

$$\varepsilon_S = |\varepsilon_G/(1 + 0.5\varepsilon_G) - 3\varepsilon_a|$$

where $\varepsilon_a = 1/a \cdot \partial a/\partial c$ is the atomic size misfit parameter, $a \approx 0.361$ nm is the lattice constant of the solvent matrix acquired from the XRD result (Fig. 1(a)), $\partial a/\partial c$ is calculated as 0.0528, and the ε_G could be neglected compared with ε_a [23]. Substituting all the parameters, the solid-solution strengthening is estimated as ~14.5 MPa.

Precipitates are expected to reinforce the solid solution matrix either through dislocation shearing mechanisms or the Orowan bypassing mechanism, which depends on the interactions between moving dislocations and precipitates. The shearing mechanism will be the dominant mechanism when the precipitates are small and coherent with the matrix, whereas the Orowan bypassing mechanism occurs when the precipitates are large or incoherent with the matrix [7–9,23,25]. In this work, since the B2 precipitates exhibiting a large average diameter of ~278 nm are incoherent with the FCC matrix, the Orowan bypassing mechanism should be employed to calculate the precipitation strengthening, which can be expressed as follow [23,25]:

$$\Delta\sigma_P = 0.4 \cdot M \cdot G \cdot b \frac{\ln\left(2\sqrt{2/3}\, r/b\right)}{\lambda_p \pi\sqrt{1-\nu}}$$

where $M = 3.06$ is the Taylor factor [23,25], G is the shear modulus (78.5 GPa) [25], $b \approx 0.255$ nm is the Burgers vector for the FCC structure, $r = 139$ nm is the average radius of the B2 precipitates, $\nu = 0.31$ is the Poisson's ratio for the FCC HEAs, $\lambda_P = 2\sqrt{2/3}\, r\left(\sqrt{\pi/4f} - 1\right)$ is the

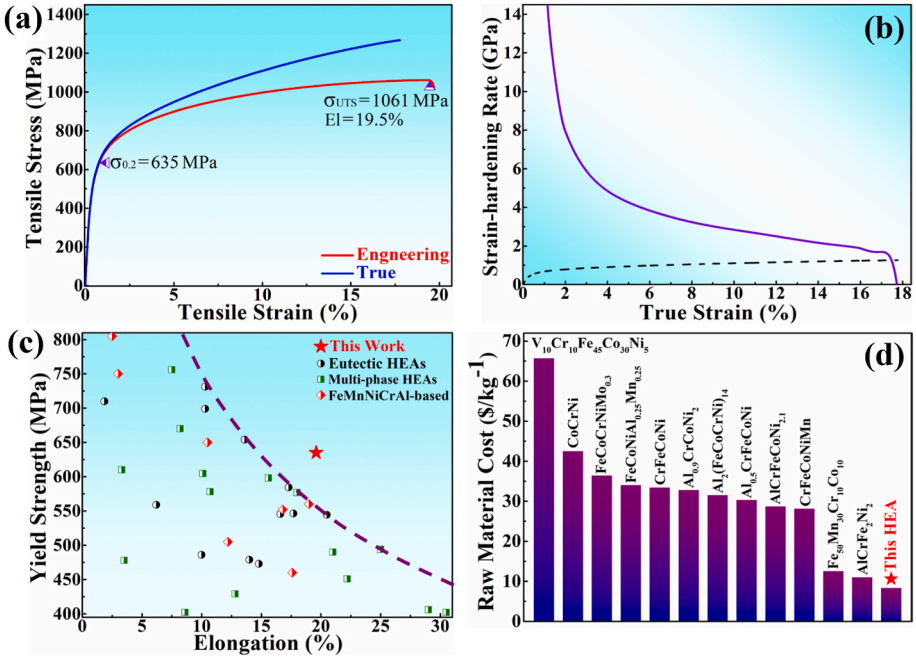

Fig. 4. Tensile properties of the as-cast $FeMn_{0.7}Ni_{0.6}Cr_{0.4}Al_{0.3}$ HEA at room temperature. (a) Representative uniaxial tensile stress-strain curves, (b) Corresponding strain hardening rate ($d\sigma^t/d\varepsilon^t$) versus true strain (ε^t) curve, (c) Tensile yield strength versus elongation in comparison with the as-cast HEAs reported in the literatures, (d) Raw material cost comparison of several HEAs, showing the lower cost of current alloy.

inter-precipitate spacing, and $f = 8.97\%$ is the volume fraction of the B2 precipitates in FCC lamellae. Thus, the particle hardening effect of B2 precipitates ($\Delta\sigma_P$) is estimated to be ~136.2 MPa. Based on the above equations, the calculated yield strength of FCC lamellae is ~699.3 MPa, which is in reasonable agreement with the experimentally observed overall yield strength of 635 MPa, albeit with some deviation.

Fig. 4(c) compares the tensile properties ($\sigma^e_{0.2}$/El^e) of typical eutectic HEAs [15,18,26–28], non-equiatomic FeMnNiCrAl HEAs [9–12], and several multi-phase HEAs [25,29–31] fabricated by casting methods. Evidently, the $FeMn_{0.7}Ni_{0.6}Cr_{0.4}Al_{0.3}$ alloy shows the best tensile properties among all the above-mentioned alloys, indicating that FCC/BCC lamellar structure has significantly enhanced strength and ductility simultaneously. Moreover, Fig. 4(d) represents the raw material cost of some previously developed high-performance HEAs. The HEAs' raw material cost was estimated by summing the prices of the constituent elements. The prices of elements were obtained from the website https://www.metal.com/price/. Undoubtedly, the studied alloy fabricated with relatively cheap components (Fe and Mn) is much more economical than the other HEAs owing to the removal of costly Co element. In addition, as the tensile strength and ductility were obtained for the as-cast state, thermo-mechanical processing and/or heat treatment could be used to optimize the microstructure and thereby further enhance the mechanical properties of this alloy. Therefore, the studied Co-free $FeMn_{0.7}Ni_{0.6}Cr_{0.4}Al_{0.3}$ HEA has successfully achieved an excellent combination of high-performance and cost-effectiveness, offering great potential for engineering applications.

4. Conclusion

In conclusion, a novel cost-effective $FeMn_{0.7}Ni_{0.6}Cr_{0.4}Al_{0.3}$ HEA with outstanding mechanical properties was successfully designed and prepared by conventional melting method. The alloy was composed of alternating lamellae with disordered FCC and disordered BCC structure, with a few ordered Ni, Al-enriched BCC (B2) precipitates embedded in the Al, Cr-depleted FCC matrix and high-density of B2 precipitates embedded in the Fe, Cr-enriched BCC matrix homogeneously. The as-cast HEA possesses a superior strength-ductility combination, i.e., a yield strength of ~635 MPa, an ultimate strength of ~1061 MPa, and total elongation of ~19.4% at room temperature, which could be primarily attributed to the lamellar boundary strengthening. The excellent as-cast properties and low-cost advantage render this alloy strong possibility to manufacture high-performance metallic products by direct casting.

CRediT authorship contribution statement

Zhenfei Jiang: Writing – original draft, Validation, Software, Methodology, Investigation, Data curation. **Weiping Chen:** Supervision, Project administration, Funding acquisition. **Chenliang Chu:** Validation, Software, Methodology. **Zhiqiang Fu:** Writing – review & editing, Supervision, Project administration, Funding acquisition. **Yemao Lu:** Writing – review & editing, Supervision, Resources, Funding acquisition. **Yulia Ivanisenko:** Writing – review & editing, Supervision, Project administration.

Declaration of competing interest

The authors declare that they have no known competing financial interests or personal relationships that could have appeared to influence the work reported in this paper.

Data availability

Data will be made available on request.

Acknowledgements

The authors acknowledge the financial support by the Key-Area Research and Development Program of Guangdong Province (Grant No. 2018B090905002), the National Natural Science Foundation of China (Grant No. 52103360 and No. 52271029), and the Basic Research Foundation of Guangzhou City (Grant No. 201804020071). The experimental support of Sinoma Institute of Materials Research (Guang Zhou) Co., Ltd and the Karlsruhe Nano Micro Facility (KNMF), a Helmholtz Research Infrastructure at Karlsruhe Institute of Technology is gratefully acknowledged.

References

[1] J.W. Yeh, S.K. Chen, S.J. Lin, J.Y. Gan, T.S. Chin, T.T. Shun, C.H. Tsau, S.Y. Chang, Nanostructured high-entropy alloys with multiple principal elements: novel alloy design concepts and outcomes, Adv. Eng. Mater. 6 (2004) 299–303.
[2] B. Cantor, I.T.H. Chang, P. Knight, A.J.B. Vincent, Microstructural development in equiatomic multicomponent alloys, Mater. Sci. Eng. A. 375–377 (2004) 213–218.
[3] C.J. Liang, C.L. Wang, M.L. Liang, Y.G. Xie, W.J. Liu, J.J. Yang, X. Li, C. Liu, S. F. Zhou, Effect of different durations on the microstructure and tribological behavior of $(Co_{1.5}FeNi)_{90}Ti_6Al_4$ high entropy alloy, Vacuum 195 (2022), 110677.
[4] L. Han, F. Maccari, I.R.S. Filho, Ni.J. Peter, Y. Wei, B. Gault, O. Gutfleisch, Z. Li, D. Raabe, A mechanically strong and ductile soft magnet with extremely low coercivity, Nature 608 (2022) 310–316.
[5] I. Solodkyi, S. Teslia, O. Bezdorozhev, I. Trosnikova, O. Yurkova, I. Bogomol, P. Loboda, Hardmetals prepared from WC-W_2C eutectic particles and AlCrFeCoNiV high entropy alloy as a binder, Vacuum 195 (2022), 110630.
[6] T. Yang, Y.L. Zhao, Y. Tong, Z.B. Jiao, J. Wei, J.X. Cai, X.D. Han, D. Chen, A. Hu, J. J. Kai, K. Lu, Y. Liu, C.T. Liu, Multicomponent intermetallic nanoparticles and superb mechanical behaviors of complex alloys, Science 362 (2018) 933–937.
[7] J. Zhou, H. Liao, H. Chen, A. Huang, Microstructure and tensile mechanical behavior of a single-phase $Fe_{35}Mn_{10}Cr_{20}Ni_{35}$ high-entropy alloy, J. Mater. Eng. Perform. 30 (2021) 3352–3362.
[8] J. Fan, L. Fu, Y. Sun, F. Xu, Y. Ding, M. Wen, A. Shan, Unveiling the precipitation behavior and mechanical properties of Co-free $Ni_{47-x}Fe_{30}Cr_{12}Mn_8Al_xTi_3$ high-entropy alloys, J. Mater. Sci. Technol. 118 (2022) 25–34.
[9] Y.L. Zhao, T. Yang, J.H. Zhu, D. Chen, Y. Yang, A. Hu, C.T. Liu, J.J. Kai, Development of high-strength Co-free high-entropy alloys hardened by nanosized precipitates, Scripta Mater. 148 (2018) 51–55.
[10] Y. Wu, X. Jin, M. Zhang, H. Yang, J. Qiao, Y. Wu, Yield strength-ductility trade-off breakthrough in Co-free $Fe_{40}Mn_{10}Cr_{25}Ni_{25}$ high-entropy alloys with partial recrystallization, Mater. Today Commun. 28 (2021), 102718.
[11] D. Shaysultanov, G. Salishchev, Y.V. Ivanisenko, S. Zherebtsov, M. Tikhonovsky, N. Stepanov, Novel $Fe_{36}Mn_{21}Cr_{18}Ni_{15}Al_{10}$ high entropy alloy with bcc/B2 dual-phase structure, J. Alloys Compd. 705 (2017) 756–763.
[12] T. Nguyen, M. Huang, H. Li, L. Hong, S. Yang, Effect of Al content on microstructure and mechanical properties of as-cast $Al_xFeMnNiCrCu_{0.5}$ high-entropy alloys, Mater. Sci. Eng. A. 832 (2022), 142495.
[13] R. Guo, J. Pan, L. Liu, Achieving dual-phase structure and improved mechanical properties in $AlCoCrFeTi_{0.5}$ high-entropy alloys by addition of Ni, Mater. Sci. Eng. A. 831 (2022).
[14] X. Gu, D. Huang, Y. Zhuang, Significant evolutions of microstructure and mechanical properties of $Al_{0.3}CoCrFeNiTi_x$ high-entropy alloys under annealing treatment, Vacuum 204 (2022), 111350.
[15] Y. Lu, X. Gao, L. Jiang, Z. Chen, T. Wang, J. Jie, H. Kang, Y. Zhang, S. Guo, H. Ruan, Y. Zhao, Z. Cao, T. Li, Directly cast bulk eutectic and near-eutectic high entropy alloys with balanced strength and ductility in a wide temperature range, Acta Mater. 124 (2017) 143–150.
[16] Y. Xiao, X. Peng, T. Fu, A novel high performance eutectic medium-entropy alloy with nanoprecipitates, Vacuum 200 (2022), 111017.
[17] Z. Jiang, W. Chen, Z. Xia, W. Xiong, Z. Fu, Influence of synthesis method on microstructure and mechanical behavior of Co-free AlCrFeNi medium-entropy alloy, Intermetallics 108 (2019) 45–54.
[18] H. Jiang, D. Qiao, W. Jiao, K. Han, L. Yiping, P.K. Liaw, Tensile deformation behavior and mechanical properties of a bulk cast $Al_{0.9}CoFeNi_2$ eutectic high-entropy alloy, J. Mater. Sci. Technol. 61 (2021) 119–124.
[19] I. Gutierrez-Urrutia, D. Raabe, Dislocation and twin substructure evolution during strain hardening of an Fe-22 wt.% Mn-0.6 wt.% C TWIP steel observed by electron channeling contrast imaging, Acta Mater. 59 (2011) 6449–6462.
[20] I. Baker, F. Meng, Lamellar coarsening in $Fe_{28}Ni_{18}Mn_{33}Al_{21}$ and its influence on room temperature tensile behavior, Acta Mater. 95 (2015) 124–131.
[21] L. Fan, T. Yang, Y. Zhao, J. Luan, G. Zhou, H. Wang, Z. Jiao, C.T. Liu, Ultrahigh strength and ductility in newly developed materials with coherent nanolamellar architectures, Nat. Commun. 11 (2020) 1–8.
[22] J. Ren, Y. Zhang, D. Zhao, Y. Chen, S. Guan, Y. Liu, L. Liu, S. Peng, F. Kong, J. D. Poplawsky, G. Gao, T. Voisin, K. An, Y.M. Wang, K.Y. Xie, T. Zhu, W. Chen, Strong yet ductile nanolamellar high-entropy alloys by additive manufacturing, Nature 608 (2022) 62–68.
[23] T. Lu, T. He, P. Zhao, K. Sun, A.F. Andreoli, H. Chen, W. Chen, Z. Fu, S. Scudino, Fine tuning in-sync the mechanical and magnetic properties of $FeCoNiAl_{0.25}Mn_{0.25}$

high-entropy alloy through cold rolling and annealing treatment, J. Mater. Process. Technol. 289 (2021), 116945.
[24] F. Otto, A. Dlouhý, C. Somsen, H. Bei, G. Eggeler, E.P. George, The influences of temperature and microstructure on the tensile properties of a CoCrFeMnNi high-entropy alloy, Acta Mater. 61 (2013) 5743–5755.
[25] Y. Ma, Q. Wang, B.B. Jiang, C.L. Li, J.M. Hao, X.N. Li, C. Dong, T.G. Nieh, Controlled formation of coherent cuboidal nanoprecipitates in body-centered cubic high-entropy alloys based on $Al_2(Ni,Co,Fe,Cr)_{14}$ compositions, Acta Mater. 147 (2018) 213–225.
[26] X. Jin, Y. Zhou, L. Zhang, X. Du, B. Li, A new pseudo binary strategy to design eutectic high entropy alloys using mixing enthalpy and valence electron concentration, Mater. Des. 143 (2018) 49–55.
[27] Q. Liu, X. Liu, X. Fan, R. Li, X. Tong, P. Yu, G. Li, Designing novel AlCoCrNi eutectic high entropy alloys, J. Alloys Compd. 904 (2022), 163775.
[28] P. Shi, Y. Li, Y. Wen, Y. Li, Y. Wang, W. Ren, T. Zheng, Y. Guo, L. Hou, Z. Shen, Y. Jiang, J. Peng, P. Hu, N. Liang, Q. Liu, P.K. Liaw, Y. Zhong, A precipitate-free AlCoFeNi eutectic high-entropy alloy with strong strain hardening, J. Mater. Sci. Technol. 89 (2021) 88–96.
[29] G. Qin, R. Chen, P.K. Liaw, Y. Gao, L. Wang, Y. Su, H. Ding, J. Guo, X. Li, An as-cast high-entropy alloy with remarkable mechanical properties strengthened by nanometer precipitates, Nanoscale 12 (2020) 3965–3976.
[30] Y.J. Liang, L. Wang, Y. Wen, B. Cheng, Q. Wu, T. Cao, Q. Xiao, Y. Xue, G. Sha, Y. Wang, Y. Ren, X. Li, L. Wang, F. Wang, H. Cai, High-content ductile coherent nanoprecipitates achieve ultrastrong high-entropy alloys, Nat. Commun. 9 (2018) 1–8.
[31] Y. Ji, L. Zhang, X. Lu, H. Fu, Z. Zhu, H. Li, H. Zhang, H. Zhang, Microstructure and tensile properties of Co-free $Fe_4CrNi(AlTi)_x$ high-entropy alloys, Intermetallics 138 (2021) 1–8.